

Hemodynamic changes in a middle cerebral artery aneurysm at follow-up times before and after its rupture: a case report and a review of the literature

A. Sejkorová^{1,2} · K. D. Dennis² · H. Švihlová³ · O. Petr⁴ · G. Lanzino⁵ · A. Hejčl^{1,6} · D. Dragomir-Daescu⁷

Received: 20 July 2016 / Revised: 3 October 2016 / Accepted: 17 October 2016 / Published online: 24 November 2016
© Springer-Verlag Berlin Heidelberg 2016

Abstract Hemodynamic parameters play a significant role in the development of cerebral aneurysms. Parameters such as wall shear stress (WSS) or velocity could change in time and may contribute to aneurysm growth and rupture. However, the hemodynamic changes at the rupture location remain unclear because it is difficult to obtain data prior to rupture. We analyzed a case of a ruptured middle cerebral artery (MCA) aneurysm for which we acquired imaging data at three time points, including at rupture. A patient with an observed MCA aneurysm was admitted to the emergency department with clinical symptoms of a subarachnoid hemorrhage. During three-dimensional (3D) digital subtraction angiography (DSA), the aneurysm ruptured again. Imaging data from two visits before rupture and this 3D DSA images at the moment of rupture were acquired, and computational fluid dynamic (CFD) simulations were performed. Results were used to describe the time-dependent changes of the hemodynamic

variables associated with rupture. Time-dependent hemodynamic changes at the rupture location were characterized by decreased WSS and flow velocity magnitude. The impingement jet in the dome changed its position in time and the impingement area at follow-up moved near the rupture location. The results suggest that the increased WSS on the dome and increased low wall shear stress area (LSA) and decreased WSS on the daughter bleb with slower flow and slow vortex may be associated with rupture. CFD performed during the follow-up period may be part of diagnostic tools used to determine the risk of aneurysm rupture.

Keywords Computational fluid dynamics · Flow dynamic · Rupture location · Velocity · Wall shear stress

Introduction

In daily practice, neurosurgeons who need to decide to pursue either intervention or conservative therapy for patients with unruptured cerebral aneurysms must rely mainly on certain clinical and morphological factors such as localization, shape, size, or sex, which may be indicative of rupture risk [26, 41, 50, 54].

Hemodynamics in cerebral vessels play a substantial role in the development of intracranial aneurysms and could be one of the causes of aneurysm rupture [8, 28, 55]. The value of hemodynamic variables such as velocity in the dome and wall shear stress (WSS) distribution on the aneurysm wall may change in time, and these changes may contribute to an increased risk of aneurysm rupture. Time-dependent changes of characteristic hemodynamic patterns at the aneurysm dome and at the rupture location remain unclear because it is difficult to obtain data before rupture.

✉ D. Dragomir-Daescu
DragomirDaescu.Dan@mayo.edu

¹ Department of Neurosurgery, Masaryk Hospital, J. E. Purkyně University, Ústí nad Labem, Czech Republic

² Division of Engineering, Mayo Clinic, Rochester, MN, USA

³ Mathematical Institute of Charles University, 8, Praha, Czech Republic

⁴ Department of Neurosurgery, Medical University Innsbruck, Innsbruck, Austria

⁵ Department of Neurological Surgery, Mayo Clinic, Rochester, MN, USA

⁶ International Clinical Research Center, St. Anne's University Hospital, Brno, Czech Republic

⁷ Department of Physiology and Biomedical Engineering, Mayo Clinic, 200 1st St SW, Rochester, MN 55905, USA

We observed a rare case of a middle cerebral artery (MCA) aneurysm during its rupture and obtained real-time imaging of rebleeding. We also acquired computed tomography angiography (CTA) data at first diagnostic in 2005, the last CTA before rupture in 2009, and 3D digital subtraction angiography (DSA) after aneurysm rupture in 2011. Computational fluid dynamic (CFD) simulations of the MCA aneurysm were performed to characterize time-dependent changes of the hemodynamic variables associated with the aneurysm rupture. A review of literature about CFD in MCA was also performed.

Materials and methods

Patient

A 53-year-old woman was diagnosed with nasopharyngeal carcinoma (WHO III), clinical stage IIB (T1, N1, M0), and has undergone modulated radiation therapy and received three rounds of adjuvant chemotherapy. In 2005, during the process of primary diagnosis, the first obtained CTA of the head showed a 4–5-mm unruptured and asymptomatic aneurysm of the right MCA in the trifurcation. Subsequent CTA after 5 months at the neurological surgery department showed an enlarged bilobed MCA aneurysm. At this time, the patient declined the DSA examination and possible treatment because of poor condition after chemotherapy. It was decided to follow-through with CTA and DSA in 3 months. After 4 months, an attempt was made at coiling, but the aneurysm was found not to be amenable to coiling. The patient was followed-through with CTA for the next 4 years. Conservative therapy was chosen because of the possible recurrence of nasopharyngeal carcinoma and the clinical state of the patient. After 5 years and 4 months from the first consultation, the patient was found fallen at work and was transferred to the emergency department for evaluation. She was awake, alert, but confused, without local neurological deficit. She underwent a head CT which revealed diffuse subarachnoid hemorrhage. She was taken urgently to angiography for potential coiling. During coil embolization, a perforation of the aneurysm occurred, which was controlled by the coil therapy. Following the procedure, a head CT revealed a clot in the right frontotemporal region (Fig. 1). The patient was subsequently taken to the operating room for an emergent bone flap craniotomy for clot removal and external ventricular drain placement. The patient recovered and regularly visits the attending neurosurgeon.

Imaging data and hemodynamic modeling

This case report was conducted with patient consent for the use of imaging and clinical data. Hemodynamic aneurysm modeling was performed as previously described by Hodis et al. [24]. Briefly, the raw imaging data for the first diagnostic CTA

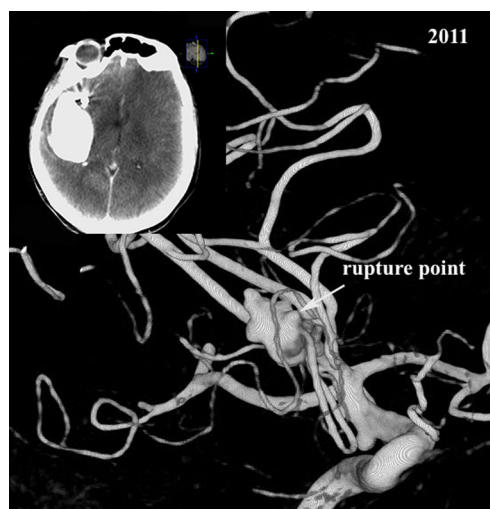


Fig. 1 Images of an MCA aneurysm from 3D DSA at time of the aneurysm rupture and from CT after the aneurysm rupture. Inset CT image shows a clot in the frontotemporal region and the aneurysm packed with coils

examination (2005) and the last CTA examination before aneurysm rupture (2009) were obtained from the Digital Imaging and Communications in Medicine (DICOM) file. The images from 3D DSA at the moment of rebleeding, but before coiling (2011), were exported as a stereolithography (STL) file. The STL file for the third model and two DICOM file sets for the first two models were imported into the software Mimics 16.0

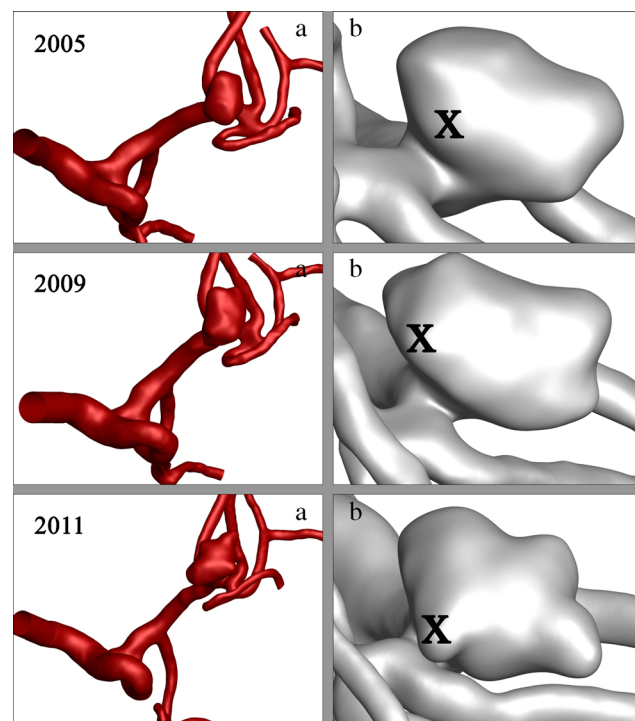


Fig. 2 Aneurysm morphology. **a** Overview of the aneurysm models in 2005, 2009, and 2011 with **b** a detail on the aneurysm dome showing the rupture location (x)

Table 1 Morphological parameters

Year	Aneurysm size (mm)	Neck width (mm)	Aspect ratio	Maximal height (mm)
2005	4.75	5.67	0.838	5.79
2009	5.13	6.26	0.819	6.85
2011	4.71	6.42	0.734	7.80

(Materialise, Leuven, Belgium) to segment geometries and obtain the 3D models. The artery inlet was cut at the same locations for all three models and was the longest available in all models. Using ICEM CFD (ANSYS, Canonsburg, PA, USA), a high-quality hexahedral grid was constructed including inflation layers to model the boundary layer near the wall. The thickness of the first inflation layer was set to 0.01 mm and an inflation factor ratio of 1.2 was used for the successive layers. The size of the final layer matched the size of the hexahedral grid in the model's core.

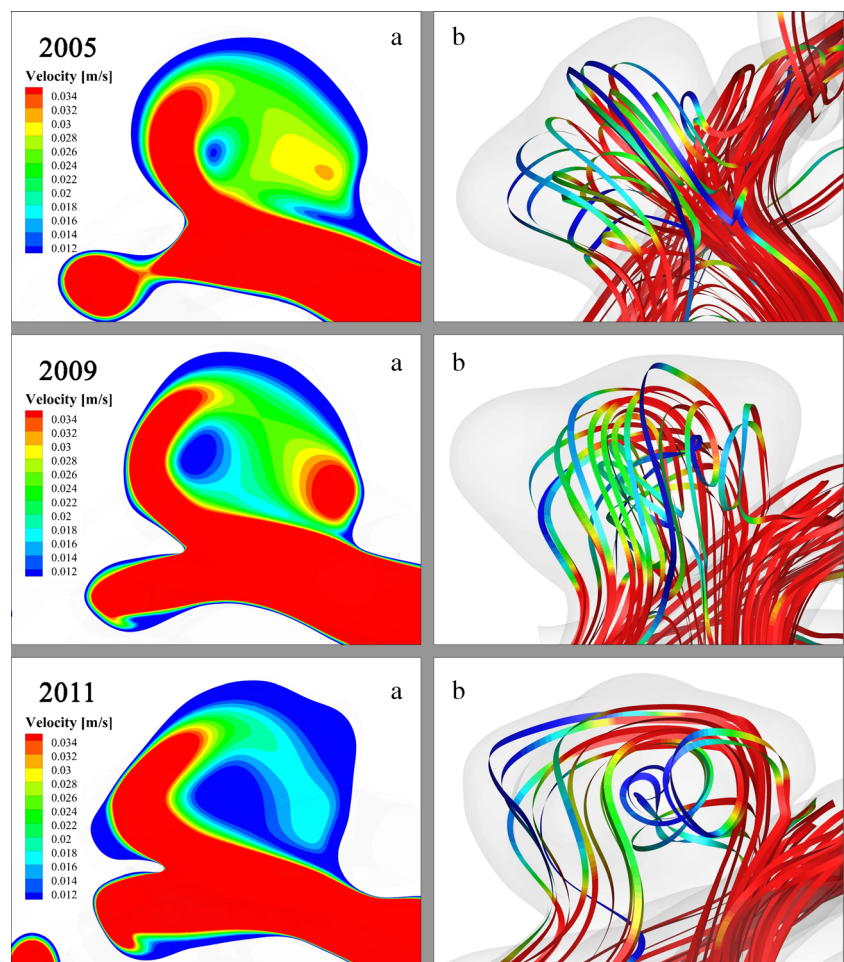
A grid sensitivity study was conducted in order to obtain an accurate grid-independent solution [25]. Simulations were based on the finest grid with a maximum element size of 0.1 mm,

resulting in grids of roughly 7–12 million elements, dependent on particular visit model. The software ANSYS Fluent 16.1 was used for simulations of hemodynamics and for generating the solution. The blood was assumed homogeneous and incompressible in a laminar flow condition. The blood vessel wall was assumed to be rigid with no-slip boundary condition. A density of 1050 kg/m^3 and a dynamic viscosity of 0.0035 Pa/s were specified for each simulation. A pulsatile Womersley velocity profile was prescribed at the inlets. Zero-pressure boundary conditions were set at all outlets. Four cardiac cycle simulations with a period of 1 s were performed. The results from the fourth cardiac cycle were used for the final analyses.

Data analysis

Aneurysm morphological characteristics such as aneurysm size (largest perpendicular distance between the neck plane and aneurysm dome), maximal height (largest distance between the neck center and aneurysm surface), aspect ratio (AR) (the ratio of the maximum perpendicular height to the average neck diameter), and neck width (twice the average

Fig. 3 Visualization of intra-aneurysm flow at peak systole. **a** Velocity contours show the flow direction. The single inflow jet impinges on the proximal aneurysm wall creating a small impingement area. **b** *Streaklines*, colored by velocity magnitude, show the complex flow pattern with a single vortex inside the aneurysm. Between 2005 and 2009, the inflow jet is moving more towards the future rupture location. In 2011, the direction of the inflow jet did not change through the cardiac cycle



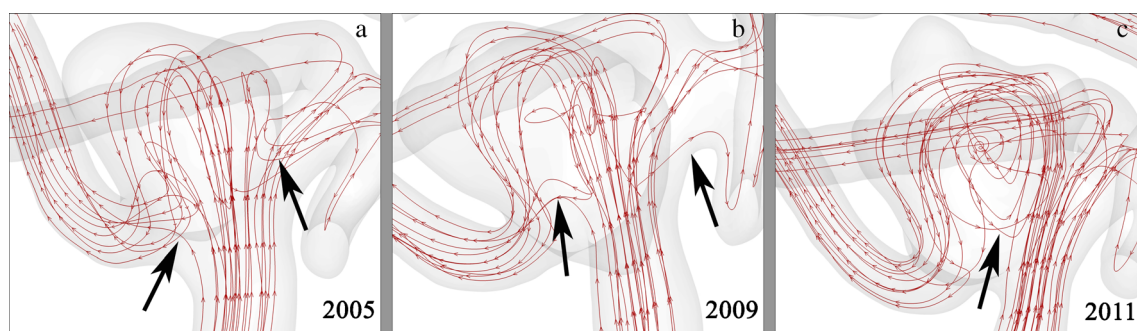


Fig. 4 Streamline distributions at peak systole. In 2005 and 2009, the inflow from the parent artery was divided into two outflow arteries (arrows). In 2011, the flow from the parent artery continued to the

artery in the direction of the parent artery and inside the aneurysm creating single vortex, which is the source of blood flow in the second outflow artery (arrow)

distance from the neck centroid to the edge of the neck) were evaluated as described by Dhar et al. [15] and Raghavan et al. [41]. The rupture location was identified on 3D DSA images (Fig. 1). To report hemodynamic results, the aneurysm dome (surface and volume of the aneurysm defined by the aneurysm neck) and a bleb where the bleeding occurred were separated from overall vasculature during geometry reconstruction for CFD analysis (Fig. 2). The bleb was considered well defined because the neck of the bleb was easily recognizable visually [9]. Hemodynamic variables such as WSS, velocity, pressure, and oscillatory shear index (OSI) were defined as previously described [7, 10, 22, 28, 36, 44, 55]. Mean WSS distributions were normalized by the average parent vessel WSS to obtain normalized WSS [28]. Low wall shear stress area (LSA) was defined as the areas of the aneurysm wall exposed to a WSS value below 10% of the mean parent vessel (the artery region from the last bifurcation upstream of the aneurysms to the aneurysm neck) WSS value [28, 55]. Mean magnitude values of velocity, pressure, WSS, WSS maximum and minimum values, normalized WSS and LSA values at peak systole and time-average values of mean WSS magnitude (TAWSS), TAWSS maximum and minimum values, normalized TAWSS, LSA averaged over the whole cardiac cycle, and OSI were calculated for the aneurysm dome and the ruptured bleb. All parameters were visualized using the software Tecplot 360 (Tecplot Inc., Bellevue, WA, USA). The intra-aneurysmal flow velocity patterns were visualized as time-dependent variables through the fourth cardiac cycle and were classified and described according to Cebal et al. [7]. Tecplot was used to define the number of vortices inside the aneurysm and to visualize the flowlines.

Results

Table 1 shows the values of morphological parameters. The maximal height grew by 35% showing the enlargement tendency of the aneurysm. The largest growth occurred in the two new daughter blebs, of which one ruptured (Fig. 3). Between 2005

and 2009, the aneurysm size and neck width grew. The value of AR decreased as the neck diameter increased. The progressive course of growth continued between 2009 and 2011. After rupture, the neck width was larger; however, the values of aneurysm size and AR both decreased. The rupture location was confirmed by a neurosurgeon (GL) and was defined from the DSA images as the bleb location with leaking blood.

The aneurysm can be described as a “parallel” [48] type with the inflow jet in the direction of the parent artery flow. The velocity patterns based on 3D streamlines and streaklines of intra-aneurysmal flow during the fourth 1-s cardiac cycle

Table 2 Hemodynamic parameters—systolic peak values

Variables	Localization	Year		
		2005	2009	2011
Mean WSS (Pa)	Dome	0.186	0.228	0.251
	Parent vessel	0.864	0.785	1.383
	Rupture location	0.236	0.130	0.745
Max WSS (Pa)	Dome	4.126	10.598	11.412
	Rupture location	1.761	0.790	5.677
Min WSS (Pa)	Dome	0.007	0.0001	0.002
	Rupture location	0.110	0.350	0.086
Normalized WSS	Dome	0.216	0.290	0.182
	Rupture location	0.273	0.166	0.539
LSA (%)	Dome	40.6	37.4	61.9
	Rupture location	0	50.6	2.0
Mean velocity (m/s)	Dome	0.0219	0.0231	0.0230
	Rupture location	0.0148	0.0088	0.0496
Max velocity (m/s)	Dome	0.1250	0.1654	0.2330
	Rupture location	0.0645	0.0432	0.1710
Mean pressure (Pa)	Dome	58.3	60.2	43.9
	Rupture location	58.1	59.7	47.6
Max pressure (Pa)	Dome	63.5	70.5	65.8
	Rupture location	59.3	60.6	51.8

Max maximum, *Min* minimum, WSS wall shear stress, LSA low wall shear stress area proportion

showed that the unruptured aneurysm had a complex flow pattern. The direction of the inflow jet and the impingement area both changed through the cardiac cycle while a large vortex existed inside the aneurysm dome along with another smaller slower vortex that developed in the daughter bleb which will rupture later in 2011 (Fig. 4a, b) [7]. The impingement of the single small inflow jet on the proximal aneurysm wall occurred between the rupture location and the growing bleb and moved more towards the future rupture location at the end of the cardiac cycle. These intra-cardiac cycle changes were more distinctive in 2009. In 2011, the small vortex merged with the main vortex and the main vortex shifted to the zone of the daughter bleb, which ruptured, and the direction of the inflow jet did not change anymore through the cardiac cycle (Fig. 4c). The outflow in the ruptured aneurysm changed compared to the unruptured aneurysm. At rupture, the flow from the parent artery was no more divided into the two outflow arteries and aneurysm, but it continued to the

artery in the direction of the parent artery and into the aneurysm. The blood in the second outflow artery came mostly from the vortex inside the dome (Fig. 4c).

Values of hemodynamic parameters at peak systole are shown in Table 2 and their distribution is visualized in Fig. 5. Between 2005 and 2009, at peak systole, the mean WSS at the rupture location decreased by 45% and the normalized WSS decreased by 39%. In 2005, the mean WSS at the rupture location was 27% larger while in 2009 was 43% smaller than the mean WSS on the dome. LSA at the rupture location rose from 0 to 51% while at the dome remained at 40%. Pressure increased by 3% at the rupture location and at the dome. The mean velocity magnitude decreased by 41% at the rupture location.

In 2011, the mean WSS at the rupture location was 473% larger than in 2009 and the mean velocity magnitude in the daughter bleb, which ruptured, increased by 464%. LSA at the dome rose to 62 % and at the rupture location decreased to 2%

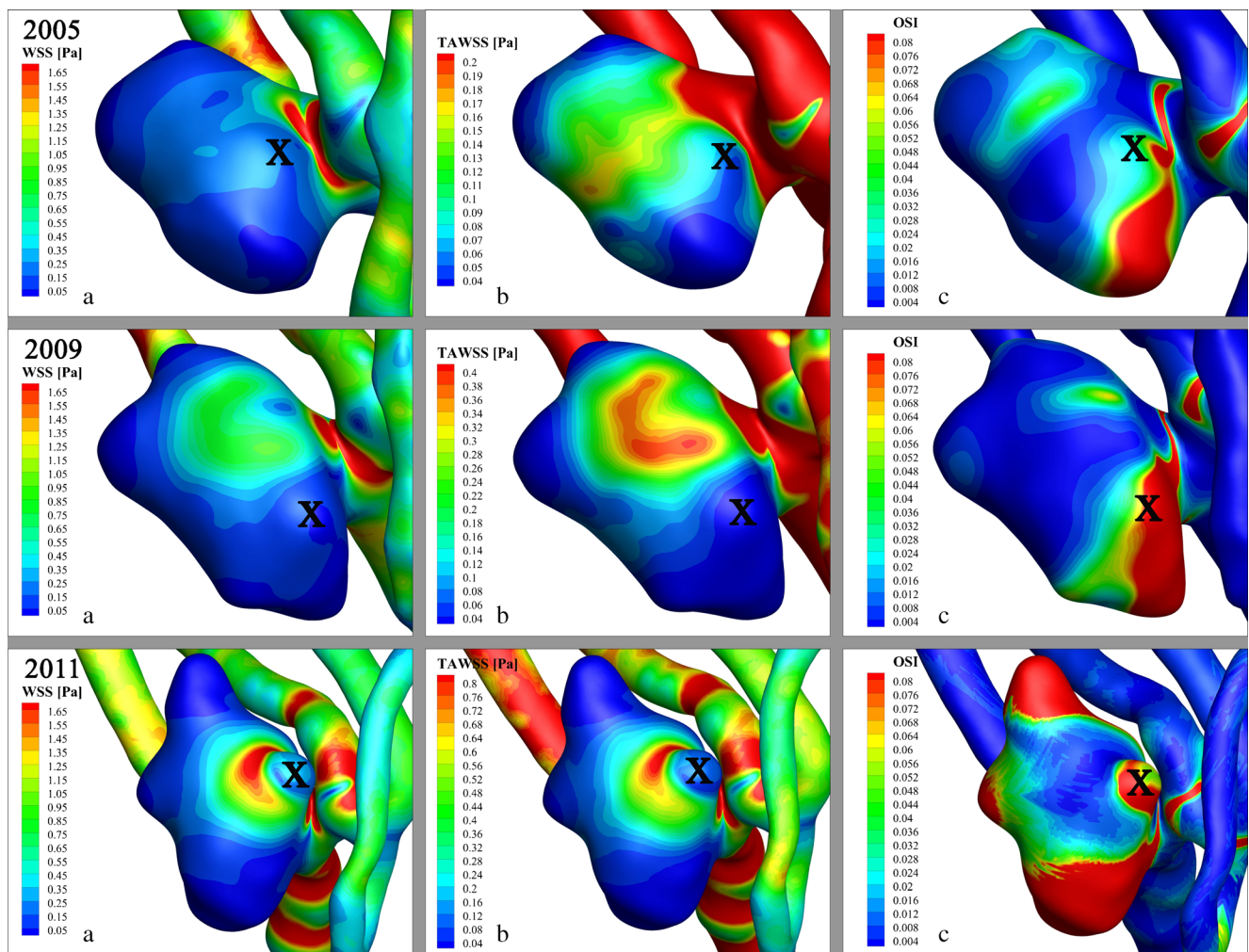


Fig. 5 WSS, TAWSS, and OSI distributions. **a** The distribution of WSS on the aneurysm dome at peak systole and **b** the distribution of TAWSS showed that WSS near and at the rupture point decreased between 2005 and 2009 while at the time of rupture in 2011 significantly increased. **c**

Between 2005 and 2009, OSI increased on the dome and at the rupture location. In 2011, OSI remained constant at the rupture location while on the dome increased substantially. X marks the rupture location

of rupture location area. Compared to values in 2009, the pressure at the rupture location and at the dome decreased by 20 and 27%, respectively.

TAWSS and the normalized TAWSS on the dome and at the rupture location showed the same tendencies as the values at peak systole (Table 3). Between 2005 and 2009, OSI increased by 105% on the dome and by 91% at the rupture location. After rupture, OSI remained constant at the rupture location while it increased substantially by 170% on the dome.

Discussion

Our study was based on the prerule imaging of an aneurysm at the times of two visits and one set of images at the moment of rupture. This study has demonstrated the possible role of time-dependent changes of hemodynamic parameters in aneurysm rupture. Between the initial diagnosis and rupture times, we observed an unstable complex flow pattern with a changing impingement region moving towards the future rupture location, a decreasing WSS and velocity magnitude at one daughter bleb, which ruptured, and a substantial increase of WSS on the aneurysm dome.

The aneurysm size and shape are parameters which are used by clinicians to determinate the aneurysm rupture risk. During the follow-up period for small unruptured aneurysms, the size of the aneurysm is the deciding factor in selecting the treatment modality. Initial aneurysm size, dome/neck ratio, and multilobarity are risk factors for aneurysm growth and potentially for aneurysm rupture [1]. Aneurysm growth was shown to correlate with low WSS and complex flow patterns [2, 13].

However, Meng et al. [33] found that the high WSS could be associated with the growth and rupture. In our case, regions of low WSS were present in both growing blebs before rupture.

Prior studies demonstrated that the intra-aneurysmal flow can be associated with aneurysm rupture [7, 17, 35, 39, 48]. MCA aneurysms are a diverse group of vascular disease, and they vary in flow pattern characteristics more than aneurysms at other locations [7, 21, 48, 51, 52]. Cebral et al. [7] classified aneurysms into four categories, depending on the flow pattern complexity and stability. All flow types were also observed for MCA locations. However, aneurysms with changing direction of the inflow jet and with creation of a single vortex were the most common (43%). Aneurysms with unstable complex flow and changing impingement region could have higher rupture risk (Table 4) [7, 17, 35, 48]. In our case, the combination of a smaller slower vortex inside the ruptured daughter bleb, the unstable complex flow in the main vortex, and the low velocity magnitude at the daughter bleb that ruptured (which was shown to have an association with aneurysm rupture [17, 35, 43, 45]) could be the factors that led to aneurysm rupture.

MCA aneurysms have unique flow pattern characteristics, but the values of some hemodynamic parameters also differ from those found at other locations [10]. Chien et al. [10] performed CFD simulations on six MCA models and observed that WSS and flow rate at peak systole were higher than at other locations such as in basilar artery and anterior communicating artery aneurysms.

High WSS may initiate aneurysm formation while lower WSS may contribute to the degenerative process in the aneurysmal wall leading to cell apoptosis and resulting in aneurysm rupture [14, 31, 34, 37]. Furthermore, low WSS may contribute to the atherosclerotic process and progressive thinning of the aneurysmal wall [29, 46]. Miura et al. [35] showed in a study with 106 MCA aneurysms that WSS may be the most reliable parameter to characterize the rupture status of MCA aneurysms. Results of more studies concerning patient-specific models of ruptured MCA aneurysm showed that low WSS may play a critical role in aneurysm rupture (Table 4) [17, 19, 27, 30, 35, 39, 42, 44]. However, according Takao et al. [49], an association between rupture status and low WSS is not statistically significant.

Another marker able to predict rupture risk is OSI [55]. Wang et al. [53] postulate that a high OSI causes the growth of the daughter bleb. Li et al. [30] showed that OSI at the rupture location of an MCA aneurysm was marginally higher than on the dome after rupture. In our case, before rupture, OSI was increasing and was higher at the rupture location than on the dome. However, after rupture, OSI at the dome increased dramatically and turned out to be higher than at the rupture location, where the OSI values stayed the same as before rupture.

With ongoing research in CFD, researchers present new hemodynamic variables which can become potential parameters to predict aneurysm rupture [23, 40, 49]. In

Table 3 Hemodynamic parameters—time-average values

Variables	Localization	Year		
		2005	2009	2011
Mean TAWSS (Pa)	Dome	0.107	0.133	0.140
	Parent vessel	0.570	0.519	0.905
	Rupture location	0.099	0.065	0.316
Max TAWSS (Pa)	Dome	2.303	6.133	5.444
	Rupture location	0.583	0.375	2.066
Min TAWSS (Pa)	Dome	0.003	0.001	0.001
	Rupture location	0.041	0.016	0.060
Normalized TAWSS	Dome	0.188	0.257	0.155
	Rupture location	0.174	0.126	0.349
LSA (%)	Dome	57.4	36.3	58.7
	Rupture location	22.1	64.1	16.0
OSI	Dome	0.02396	0.04908	0.13220
	Rupture location	0.03489	0.06664	0.06694

Max maximum, Min minimum, WSS wall shear stress, LSA low wall shear stress area proportion, OSI oscillatory shear index

Table 4 Overview of published literature regarding CFD and patient-specific MCA aneurysm models

Author	No. of MCA AN	R/UR	Flow complex/simple		Hemodynamic parameters correlated with rupture status or aneurysm wall properties
			R	UR	
Shojima et al. [43, 44]	20	3/17	–		Low flow velocity
Cebral et al. [7]	14	–/–	–		Disturbed flow patterns Small impingement regions Narrow jets
Hassan et al. [21]	27	–/–	–		–
Shojima et al. [45]	14	7/7	–		–
Szikora et al. [48]	2	2/0	–		Jet flow pattern
Chien et al. [10]	6	2/4	–		–
Bowker et al. [3]	3	0/3	3/0		–
Shojima et al. [42]	1	0/1	–		Low shear magnitude ^a High shear gradient
Wang et al. [53]	1	0/1	1/0		Low WSS Large OSI ^b
Valen-Sendstad et al. [51]	1	0/1	1/0		–
Goubergrits et al. [19]	22	7/15	–		Low WSS
Omodaka et al. [39]	6	6/0	–		Low WSS
Takao et al. [49]	50	6/43	–		Lower pressure loss coefficient
Kadasi et al. [29]	12	0/12	–		Low WSS High pressure ^c
Miura et al. [35]	106	43/63	–		Low WSS Flow stagnation Complex flow
Sugiyama et al. [46]	30	0/30	–		High prolonged RRT Low WSS ^d
Valen-Sendstad et al. [52]	12	7/5	5/2	0/5	Flow fluctuations at the dome
Li et al. [30]	1	1/0	–		Low WSS Low TAWS Higher OSI
Fukazawa et al. [17]	12	12/0	11/1		Low WSS Low flow velocity Complex flow
Jing et al. [27]	36	14/22	8/6	6/16	Large AR Low WSS

MCA middle cerebral artery, AN aneurysm, R ruptured aneurysms, UR unruptured aneurysm, – data not available, TA time-average, WSS wall shear stress, AR aspect ratio

^a In the blister formation

^b At daughter saccules (blebs)

^c At thin-walled dome regions

^d Atherosclerotic changes of aneurysm wall

MCA aneurysm models, Takao et al. [49] used the pressure loss coefficient, which characterizes energy expenditure and the geometric shape of vessels, to compare the ruptured with the unruptured aneurysms. They concluded that lower values of the pressure loss coefficient in ruptured aneurysms can be associated with higher rupture risk. Sugiyama et al. [46] and Bowker et al. [3] used the relative

residence time (RRT) to identify regions of stagnation in the flow inside the aneurysms. Results showed that prolonged RRT may be one of the risk factors of the atherosclerotic changes in the aneurysm wall [46] and decreased RRT may be associated with improved replenishment of nutrients to aneurysm wall during moderate aerobic exercise [3].

Only few recent studies consider the hemodynamic of an unruptured aneurysm before rupture. To our knowledge, none of them has studied more than one imagining data set before rupture. Most previous studies compared models of ruptured and unruptured aneurysms. Cornelissen et al. [13] pointed out that the rupture itself could change aneurysm hemodynamic and that studies comparing ruptured with unruptured aneurysms should be interpreted with caution. In our case, the hemodynamic values after rupture changed dramatically. Before rupture, WSS at the rupture location stayed constantly lower than at the parent vessel. However, after rupture, WSS and velocity magnitude increased fourfold and LSA decreased to 2% of the rupture location area. In two case-control studies, it was shown that large ICA aneurysms before rupture had a more irregular aneurysm shape, a higher AR, and a lower aneurysm averaged WSS compared to control groups of unruptured aneurysms and that normalized WSS was associated with the rupture of posterior communicating artery aneurysms [16, 32]. Chien and Sayre [11] compared four posterior communicating artery aneurysms before and after rupture and found that indicators of high aneurysm rupture risk are aneurysm surface ratio, nonsphericity index, and pulsatility index.

Limitations

Firstly, using a standardized modality during patient care poses practical challenges. We did not have high frame rate 3D DSA images for all three examinations. Obtaining the vascular geometry from CTA for the 2005 and 2009 models may have an effect on the vascular model used for computational simulations [18, 38]. Manual correction in segmentation for imaging artifacts was performed by a single neurosurgeon and checked by one engineer to insure a precise 3D model. From a physician perspective, obtaining 3D DSA is not possible all the time, because this intervention has its own complications or because the clinical state of the patient does not allow the procedure [12, 20]. In this matter, the future of CFD simulations and its clinical applications depends on the possibility to accurately process data from all imagining tools (CTA, DSA, and MRA).

Secondly, a common CFD simulation limitation of using standardized input conditions needs to be addressed. A lack of patient-specific flow profile data, the assumption of rigid vessel walls, the simplifying Newtonian assumption of the blood, and the simplified outflow boundary conditions need to be addressed. However, CFD results obtained with the help of these assumptions are considered by many researchers to realistically describe in vivo hemodynamics [4–6, 47].

Finally, the time gap between examinations before and after rupture was 1.8 years (between 2009 and 2011). We can only assume that the changes in hemodynamic continued in the same direction as in previous years. Also, our conclusions

were obtained for a single patient and the results may not be easy to generalize.

Conclusion

The assessment of the rupture risk may be possible not only from aneurysm size, shape, and aneurysm location but also from an evaluation of hemodynamic parameters and their time-dependent changes at follow-up. The increased WSS on the dome and increased LSA and decreased WSS on the daughter bleb with a decreased flow velocity may indicate a higher rupture risk. However, it is necessary to study more cases of ruptured aneurysms with follow-up periods to better understand the hemodynamic causes of aneurysm rupture.

Acknowledgments We thank Susheil Uthamaraj for assistance with the CFD simulations and the result visualization and Emily Nordahl, Jaroslav Hron, and David Kallmes, M.D., for comments that greatly improved the manuscript.

Compliance with ethical standards

Funding Operational Programme Research and Development for Innovation provided financial support in the form of the European Regional Development Fund—Project FNUSA-ICRC (No. CZ.1.05/1.1.00/02.0123). It was also supported by project no. LQ1605 from the National Program of Sustainability II (MEYS CR) and by the Ministry of Education, Youth, and Sports of the Czech Republic project no. LH14054 (KONTAKT II). The sponsor had no role in the design or conduct of this research.

Conflict of interest The authors declare that they have no competing interests.

Ethical approval All procedures performed in studies involving human participants were in accordance with the ethical standards of the institutional and/or national research committee and with the 1964 Helsinki declaration and its later amendments or comparable ethical standards.

Informed consent Informed consent was obtained from the participant included in the study.

References

1. Bor AS, Tiel Groenestege AT, terBrugge KG, Agid R, Velthuis BK, Rinkel GJ, Wermer MJ (2015) Clinical, radiological, and flow-related risk factors for growth of untreated, unruptured intracranial aneurysms. *Stroke; a journal of cerebral circulation* 46:42–48
2. Bousset L, Rayz V, McCulloch C, Martin A, Acevedo-Bolton G, Lawton M, Higashida R, Smith WS, Young WL, Saloner D (2008) Aneurysm growth occurs at region of low wall shear stress. Patient-Specific Correlation of Hemodynamics and Growth in a Longitudinal Study *Stroke* 39:2997–3002
3. Bowker TJ, Watton PN, Summers PE, Byrne JV, Ventikos Y (2010) Rest versus exercise hemodynamics for middle cerebral artery

- aneurysms: a computational study. *AJNR Am J Neuroradiol* 31:317–323
4. Castro MA, Ahumada Olivares MC, Putman CM, Cebral JR (2014) Unsteady wall shear stress analysis from image-based computational fluid dynamic aneurysm models under Newtonian and Casson rheological models. *Med Biol Eng Comput* 52:827–839
 5. Castro MA, Putman CM, Cebral JR (2006) Computational fluid dynamics modeling of intracranial aneurysms: effects of parent artery segmentation on intra-aneurysmal hemodynamics. *AJNR Am J Neuroradiol* 27:1703–1709
 6. Cebral JR, Castro MA, Appanaboyina S, Putman CM, Millan D, Frangi AF (2005) Efficient pipeline for image-based patient-specific analysis of cerebral aneurysm hemodynamics: technique and sensitivity. *IEEE Trans Med Imaging* 24:457–467
 7. Cebral JR, Castro MA, Burgess JE, Pergolizzi RS, Sheridan MJ, Putman CM (2005) Characterization of cerebral aneurysms for assessing risk of rupture by using patient-specific computational hemodynamics models. *AJNR Am J Neuroradiol* 26:2550–2559
 8. Cebral JR, Mut F, Weir J, Putman C (2011) Quantitative characterization of the hemodynamic environment in ruptured and unruptured brain aneurysms. *AJNR Am J Neuroradiol* 32:145–151
 9. Cebral JR, Sheridan M, Putman CM (2010) Hemodynamics and bleb formation in intracranial aneurysms. *AJNR Am J Neuroradiol* 31:304–310
 10. Chien A, Castro MA, Tateshima S, Sayre J, Cebral J, Vinuela F (2009) Quantitative hemodynamic analysis of brain aneurysms at different locations. *AJNR Am J Neuroradiol* 30:1507–1512
 11. Chien A, Sayre J (2014) Morphologic and hemodynamic risk factors in ruptured aneurysms imaged before and after rupture. *Am J Neuroradiol* 35:2130–2135
 12. Cloft HJ, Joseph GJ, Dion JE (1999) Risk of cerebral angiography in patients with subarachnoid hemorrhage, cerebral aneurysm, and arteriovenous malformation: a meta-analysis. *Stroke* 30:317–320
 13. Cornelissen BMW, Schneiders JJ, Potters WV, Van Den Berg R, Velthuis BK, Rinkel GJE, Slump CH, VanBavel E, Majoie CBLM, Marquering HA (2015) Hemodynamic differences in intracranial aneurysms before and after rupture. *Am J Neuroradiol* 36:1927–1933
 14. D’Arcangelo D, Ambrosino V, Giannuzzo M, Gaetano C, Capogrossi MC (2006) Axl receptor activation mediates laminar shear stress anti-apoptotic effects in human endothelial cells. *Cardiovasc Res* 71:754–763
 15. Dhar S, Tremmel M, Mocco J, Kim M, Yamamoto J, Siddiqui AH, Hopkins LN, Meng H (2008) Morphology parameters for intracranial aneurysm rupture risk assessment. *Neurosurgery* 63:185–197
 16. Duan G, Lv N, Yin J, Xu J, Hong B, Xu Y, Liu J, Huang Q (2016) Morphological and hemodynamic analysis of posterior communicating artery aneurysms prone to rupture: a matched case-control study. *Journal of NeuroInterventional Surgery* 8:47–51
 17. Fukazawa K, Ishida F, Umeda Y, Miura Y, Shimosaka S, Matsushima S, Taki W, Suzuki H (2015) Using computational fluid dynamics analysis to characterize local hemodynamic features of middle cerebral artery aneurysm rupture points. *World Neurosurg* 83:80–86
 18. Geers AJ, Larrabide I, Radaelli AG, Bogunovic H, Kim M, Gratama van Andel HA, Majoie CB, VanBavel E, Frangi AF (2011) Patient-specific computational hemodynamics of intracranial aneurysms from 3d rotational angiography and ct angiography: an in vivo reproducibility study. *AJNR Am J Neuroradiol* 32:581–586
 19. Goubergrits L, Schaller J, Kertzschner U, van den Bruck N, Poethkow K, Petz C, Hege HC, Spuler A (2012) Statistical wall shear stress maps of ruptured and unruptured middle cerebral artery aneurysms. *J R Soc Interface* 9:677–688
 20. Grzyska U, Freitag J, Zeumer H (1990) Selective cerebral intraarterial DSA: complication rate and control of risk factors. *Neuroradiology* 32:296–299
 21. Hassan T, Timofeev EV, Saito T, Shimizu H, Ezura M, Matsumoto Y, Takayama K, Tominaga T, Takahashi A (2005) A proposed parent vessel geometry-based categorization of saccular intracranial aneurysms: computational flow dynamics analysis of the risk factors for lesion rupture. [erratum appears in *J Neurosurg*. 2005 dec;103(6):1110]. *J Neurosurg* 103:662–680
 22. He X, Ku DN (1996) Pulsatile flow in the human left coronary artery bifurcation: average conditions. *J Biomech Eng* 118:74–82
 23. Himburg HA, Grzybowski DM, Hazel AL, LaMack JA, Li X-M, Friedman MH (2004) Spatial comparison between wall shear stress measures and porcine arterial endothelial permeability. *Am J Physiol Heart Circ Physiol* 286:H1916–H1922
 24. Hodis S, Uthamaraj S, Lanzino G, Kallmes DF, Dragomir-Daescu D (2014) Computational fluid dynamics simulation of an anterior communicating artery ruptured during angiography. *J Neurointerv Surg* 6:e14
 25. Hodis S, Uthamaraj S, Smith AL, Dennis KD, Kallmes DF, Dragomir-Daescu D (2012) Grid convergence errors in hemodynamic solution of patient-specific cerebral aneurysms. *J Biomech* 45:2907–2913
 26. Investigators TISOUIA (1998) Unruptured intracranial aneurysms—risk of rupture and risks of surgical intervention. *N Engl J Med* 339:1725–1733
 27. Jing L, Fan J, Wang Y, Li H, Wang S, Yang X, Zhang Y (2015) Morphologic and hemodynamic analysis in the patients with multiple intracranial aneurysms: ruptured versus unruptured. *PLoS One* 10:e0132494
 28. Jou LD, Lee DH, Morsi H, Mawad ME (2008) Wall shear stress on ruptured and unruptured intracranial aneurysms at the internal carotid artery. *AJNR Am J Neuroradiol* 29:1761–1767
 29. Kadasi LM, Dent WC, Malek AM (2013) Colocalization of thin-walled dome regions with low hemodynamic wall shear stress in unruptured cerebral aneurysms. *J Neurosurg* 119:172–179
 30. Li ML, Wang YC, Liou TM, Lin CA (2014) The hemodynamics in intracranial aneurysm ruptured region with active contrast leakage during computed tomography angiography. *Comput Mech* 54:987–997
 31. Li Y-SJ, Haga JH, Chien S (2005) Molecular basis of the effects of shear stress on vascular endothelial cells. *J Biomech* 38:1949–1971
 32. Liu J, Fan J, Xiang J, Zhang Y, Yang X (2016) Hemodynamic characteristics of large unruptured internal carotid artery aneurysms prior to rupture: a case control study. *Journal of NeuroInterventional Surgery* 8:367–372
 33. Meng H, Tutino VM, Xiang J, Siddiqui A (2014) High WSS or low WSS? Complex interactions of hemodynamics with intracranial aneurysm initiation, growth, and rupture: toward a unifying hypothesis. *Am J Neuroradiol* 35:1254–1262
 34. Meng H, Wang Z, Hoi Y, Gao L, Metaxa E, Swartz DD, Kolega J (2007) Complex hemodynamics at the apex of an arterial bifurcation induces vascular remodeling resembling cerebral aneurysm initiation. *Stroke* 38:1924–1931
 35. Miura Y, Ishida F, Umeda Y, Tanemura H, Suzuki H, Matsushima S, Shimosaka S, Taki W (2013) Low wall shear stress is independently associated with the rupture status of middle cerebral artery aneurysms. *Stroke* 44:519–521
 36. Mut F, Lohner R, Chien AC, Tateshima S, Vinuela F, Putman C, Cebral JR (2011) Computational hemodynamics framework for the analysis of cerebral aneurysms. *Int J Numer Method Biomed Eng* 27:822–839
 37. Nixon AM, Gunel M, Sumpio BE (2010) The critical role of hemodynamics in the development of cerebral vascular disease. *J Neurosurg* 112:1240–1253
 38. Omodaka S, Inoue T, Funamoto K, Sugiyama S, Shimizu H, Hayase T, Takahashi A, Tominaga T (2012) Influence of surface model extraction parameter on computational fluid dynamics modeling of cerebral aneurysms. *J Biomech* 45:2355–2361

39. Omodaka S, Sugiyama S, Inoue T, Funamoto K, Fujimura M, Shimizu H, Hayase T, Takahashi A, Tominaga T (2012) Local hemodynamics at the rupture point of cerebral aneurysms determined by computational fluid dynamics analysis. *Cerebrovasc Dis* 34:121–129
40. Qian Y, Takao H, Umezu M, Murayama Y (2011) Risk analysis of unruptured aneurysms using computational fluid dynamics technology: preliminary results. *AJNR Am J Neuroradiol* 32:1948–1955
41. Raghavan ML, Ma B, Harbaugh RE (2005) Quantified aneurysm shape and rupture risk. *J Neurosurg* 102:355–362
42. Shojima M, Nemoto S, Morita A, Oshima M, Watanabe E, Saito N (2010) Role of shear stress in the blister formation of cerebral aneurysms. *Neurosurgery* 67:1268–1274
43. Shojima M, Oshima M, Takagi K, Hayakawa M, Katada K, Morita A, Kirino T (2006) Numerical simulation of the intra-aneurysmal flow dynamics. *Interv Neuroradiol* 12:49–52
44. Shojima M, Oshima M, Takagi K, Torii R, Hayakawa M, Katada K, Morita A, Kirino T (2004) Magnitude and role of wall shear stress on cerebral aneurysm: computational fluid dynamic study of 20 middle cerebral artery aneurysms. *Stroke* 35:2500–2505
45. Shojima M, Oshima M, Takagi K, Torii R, Nagata K, Shirouzu I, Morita A, Kirino T (2005) Role of the bloodstream impacting force and the local pressure elevation in the rupture of cerebral aneurysms. *Stroke* 36:1933–1938
46. Sugiyama S, Niizuma K, Nakayama T, Shimizu H, Endo H, Inoue T, Fujimura M, Ohta M, Takahashi A, Tominaga T (2013) Relative residence time prolongation in intracranial aneurysms: a possible association with atherosclerosis. *Neurosurgery* 73:767–776
47. Sun Q, Groth A, Aach T (2012) Comprehensive validation of computational fluid dynamics simulations of in-vivo blood flow in patient-specific cerebral aneurysms. *Med Phys* 39:742–754
48. Szikora I, Paal G, Ugron A, Nasztanovics F, Marosfoi M, Berentei Z, Kulcsar Z, Lee W, Bojtar I, Nyary I (2008) Impact of aneurysmal geometry on intraaneurysmal flow: a computerized flow simulation study. *Neuroradiology* 50:411–421
49. Takao H, Murayama Y, Otsuka S, Qian Y, Mohamed A, Masuda S, Yamamoto M, Abe T (2012) Hemodynamic differences between unruptured and ruptured intracranial aneurysms during observation. *Stroke* 43:1436–1439
50. Ujiie H, Tachibana H, Hiramatsu O, Hazel AL, Matsumoto T, Ogasawara Y, Nakajima H, Hori T, Takakura K, Kajiya F (1999) Effects of size and shape (aspect ratio) on the hemodynamics of saccular aneurysms: a possible index for surgical treatment of intracranial aneurysms. *Neurosurgery* 45:119
51. Valen-Sendstad K, Mardal KA, Mortensen M, Reif BA, Langtangen HP (2011) Direct numerical simulation of transitional flow in a patient-specific intracranial aneurysm. *J Biomech* 44:2826–2832
52. Valen-Sendstad K, Mardal KA, Steinman DA (2013) High-resolution CFD detects high-frequency velocity fluctuations in bifurcation, but not sidewall, aneurysms. *J Biomech* 46:402–407
53. Wang SZ, Chen JL, Ding GH, Lu G, Zhang XL (2010) Non-newtonian computational hemodynamics in two patient-specific cerebral aneurysms with daughter saccules. *J Hydrodyn* 22:639–646
54. Wiebers DO (2003) Unruptured intracranial aneurysms: natural history, clinical outcome, and risks of surgical and endovascular treatment. *Lancet* 362:103–110
55. Xiang J, Natarajan SK, Tremmel M, Ma D, Mocco J, Hopkins LN, Siddiqui AH, Levy EI, Meng H (2011) Hemodynamic-morphologic discriminants for intracranial aneurysm rupture. *Stroke* 42:144–152